Versão do arquivo anexado / Version of attached file:

Versão do Editor / Published Version

Mais informações no site da editora / Further information on publisher's website:

https://pos.sissa.it/444/238

DOI: 10.22323/1.444.0238

Search for primary photons at tens of PeV with the Pierre Auger Observatory

Nicolás González[a,*] **for the Pierre Auger Collaboration**[b]

[a]*Instituto de Tecnologías en Detección y Astropartículas (ITeDA),*
 Av. Gral Paz 1499, B1650KNA San Martín, Buenos Aires, Argentina

[b]*Observatorio Pierre Auger, Av. San Martín Norte 304, 5613 Malargüe, Argentina*
 Full author list: https://www.auger.org/archive/authors_icrc_2023.html

 E-mail: auger_spokespersons@fnal.gov

The observation of primary photons with energies around 10^{16} eV would be particularly interesting after the discovery of Galactic gamma-ray sources with spectra extending into the PeV range. Since photons are connected to the acceleration of charged particles, searches for photons enhance the multi-messenger understanding of cosmic-ray sources as well as of transient astrophysical phenomena, while offering wealthy connections to neutrino astronomy and dark matter. Additionally, diffuse photon fluxes are expected from cosmic-ray interactions with Galactic matter and background radiation fields. Previously, the energy domain between 1 PeV and 200 PeV was only explored from the Northern Hemisphere. The Pierre Auger Observatory is the largest astroparticle experiment in operation and, thanks to its location, has a sizable exposure to the Southern sky, including the Galactic center region. In this contribution, we present the first search for photons from the Southern hemisphere between 50 and 200 PeV exploiting the Auger data acquired during ~ 4 yr of operation. We describe the method to discriminate photons against the dominating hadronic background; it is based on the measurements of air showers taken with the low-energy extension of the Pierre Auger Observatory composed by 19 water-Cherenkov detectors spanning ~ 2 km^2 and an Underground Muon Detector. The search for a diffuse flux of photons is presented and its results are interpreted according to theoretical model predictions. This study extends the range of Auger photon searches to almost four decades in energy.

---

*Speaker

1. Introduction

The origin of ultra-high-energy cosmic rays remains an open problem in astroparticle physics. The cosmic-ray acceleration mechanisms can be probed through the detection of primary (astrophysical) photons generated in the vicinity of the sources. Due to the interaction with background radiation fields, primary photons with energies below 10^{18} eV can propagate through distances smaller than a few Mpc. As a result, photons are excellent probes of Galactic steady sources and transient phenomena. Recent observations have revealed the existence of primary photons up to a few PeV originating from various Galactic sources [1]. However, the precise mechanisms leading to the production of the precursor charged particles are still not fully understood due to the limited exposure above a few PeV. In addition, diffuse cosmogenic photons can be produced during the propagation of ultra-high-energy cosmic rays, either in interactions with Galactic matter [2] or with the microwave background field [3, 4]. Finally, theoretical models describing the existence of dark matter in the Galactic center predict a steady flux of primary photons above a few PeV from the decay of such exotic particles over time [5].
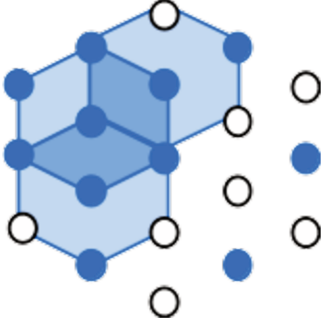

Figure 1: A schematic view of the SD-433 array. Filled blue positions are equipped with buried muon detectors. Only events acquired by the three highlighted hexagons are considered for the photon search presented here (see Sec. 2).

The most stringent limits to the integral photon flux have been established by the Pierre Auger Collaboration above 200 PeV [6]. Cosmic rays and photons initiate air showers that can be measured with arrays of ground detectors. The Pierre Auger is the largest observatory in operation, comprised of several detection systems aimed at extracting information of different particles composing the air-shower front [7]. In particular, its most dense surface detector array consisting of 19 water-Cherenkov detectors (WCDs) arranged in a grid of seven regular hexagons with a distance of 433 m between the detectors (SD-433) [8], as depicted in Fig. 1. The SD-433 can be employed to reconstruct the characteristics of the primary particle above a few tens of PeV. Alongside 11 of the WCDs, buried scintillation modules compose part of the Underground Muon Detector (UMD) which can be used to measure the number of high-energy muons arriving at the ground [9]. Since air showers initiated by photons are almost purely electromagnetic in nature, they contain fewer secondary muons compared to their hadronic counterparts. Therefore, the measured number of muons can be exploited to discriminate primary photons from the cosmic-ray background.

At energies between a few PeV and 200 PeV, upper limits to the integral photon flux exist only from Observatories located in the Northern hemisphere [10], from where the location of the Galactic plane and center is restricted. Considering the variety of open problems that can be tackled by the observation of primary photons above a few PeV, we present the first photon search from the Southern hemisphere in the energy range between 50 and 200 PeV with the data from the Pierre Auger Observatory. In Sec. 2, we describe the data selection criteria, while the discrimination method is assessed with simulations in Sec. 3. The method is applied to the search data-set in Sec. 4 before computing the upper limits to the integral photon flux.

2. Data selection

To ensure the selection of high-quality data, the stability of the data acquisition of both the WCDs and the UMD modules is evaluated to identify optimal operational periods. Then the overall exposure is determined by integrating the acceptance of each SD-433 hexagon throughout the entire observation period, as defined in Eq. 1. Each factor is described in the following paragraphs.

$$\epsilon_\gamma = \sum_{\text{hexagons}} \int_t A(t) \cos\theta \cdot u_{\text{umd}}(t) \, dt \times \int_{E_\gamma} \int_\Omega \tau_{\text{eff}}(E_\gamma, \theta) \, d\Omega dE_\gamma \tag{1}$$

The operational status of the SD-433 stations is monitored on a 1-second basis to classify them as either 'on' or 'off'. Additionally, technical issues impeding the normal data transfer were identified affecting eight out of the 19 SD stations during sixteen periods lasting between one day to one week. These periods represent in total less than 1% of the operation time. During these periods, the stations were considered as 'off'.

The effective area of a hexagon with a side length $d = 433\,\text{m}$, $A = \sqrt{3}/2 \cdot d^2$, is added to the exposure calculation when its central and either five or all six first-crown SD stations are identified as 'on'. In the former case, the area needs to be adjusted by a geometrical factor of $1/3$ to account for the missing first-crown station.

The average event rate of the SD-433 during normal operation above an energy threshold of $10^{16.7}$ eV is calculated as $\bar{F}_{\text{SD-433}} = 125\,\text{week}^{-1}\,\text{hex}^{-1}$. As the number of detected events follows a Poissonian distribution, the identification of unstable periods in the data acquisition involves searching for intervals between consecutive events acquired with N_{hex} active hexagons larger than $\ln a/(\bar{F}_{\text{SD-433}} \times N_{\text{hex}}) \sim 1 - 9$ hours, where $a = 10^{-2.5}$ is a model parameter characterizing the departure from the Poissonian distribution. Applying this selection criterion results in the exclusion of around 37 weeks out of the $221-$week span covered by the initial data-set period between January 1, 2018, and March 31, 2022.

Each UMD station is composed of three $10\,\text{m}^2$ modules. The module trigger rate under normal operation is estimated to be $\bar{F}_{\text{UMD}} = 106\,\text{week}^{-1}\,\text{hex}^{-1}$. Similar to the WCDs, unstable periods for each UMD module are identified by analyzing the time intervals between consecutive appearances in the data. If the interval exceeds $\sim 1 - 7$ hours, depending on the number of active SD-433 hexagons, it is considered an unstable period in which the module is manually tagged as 'off'. The frequency of such unstable periods varies across the UMD modules, representing between 16% and 19% of the net time after applying the SD-433 selection cut described earlier.

To have sufficient sampling of the muon footprint leading to a suitable discrimination power (see Sec. 3), a hexagon is required to possess a central UMD station with all three modules tagged as 'on' and at least $80\,\text{m}^2$ tagged as 'on' in the first-crown of UMD stations. This requirement is checked in terms of the time by the step function $u_{\text{UMD}}(t)$. Therefore, events acquired by only three of the deployed hexagons (highlighted in Fig. 1) are employed for this work.

The array trigger efficiency, τ_{eff}, for air-showers initiated by primary photons is parameterized using simulated events. The air-shower library is composed of about $15,000$ primary photons and $15,000$ primary protons with energies between $10^{16} - 10^{17.5}$ eV using EPOS-LHC as the hadronic interaction model. Each shower was reused ten times to simulate the response of the SD-433 and UMD stations with the Auger $\overline{\text{Off}}\underline{\text{line}}$ framework [11]. The trigger efficiency for various zenith

angle ranges is presented in Fig. 2. The energy-integrated trigger efficiency, weighted by a spectrum E_γ^{-3}, is convolved with the aforementioned contributions to adjust the exposure, as shown in Eq. 1. This correction is approximately 12% (less than 2%) above $E_\gamma = 10^{16.7}$ eV (10^{17} eV). To ensure a good trigger efficiency, the data-set above $E_\gamma = 10^{16.7}$ eV (refer to Sec. 3 for the definition of E_γ) and up to a zenith angle of 52° is used in this study.
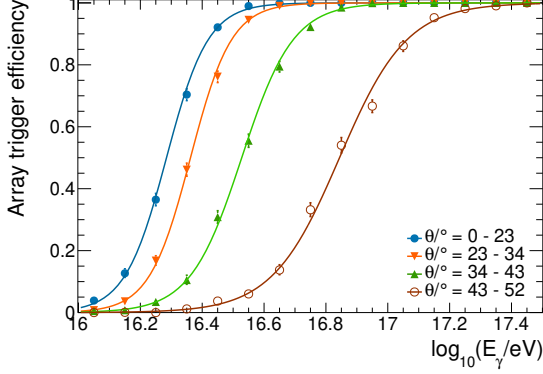

Figure 2: The trigger efficiency as a function of the simulated energy for photon primaries and different zenith angle intervals. Solid lines correspond to fitted sigmoid functions.

The selected data-set begins on December 17, 2020, when the central UMD stations of the three hexagons were deployed and operational. It extends until March 31, 2022, resulting in 15,919 recorded events during ~15.5 months. The accumulated exposure in the full-trigger-efficiency regime is $\epsilon_\gamma = 0.629\,\mathrm{km}^2$ sr yr.

3. Event-based muon estimate with M_b

The number of muons detected at ground level serves as a well-established observable for identifying air showers characterized by a dominant electromagnetic development. The high-energy muon footprint is directly measured by the UMD sta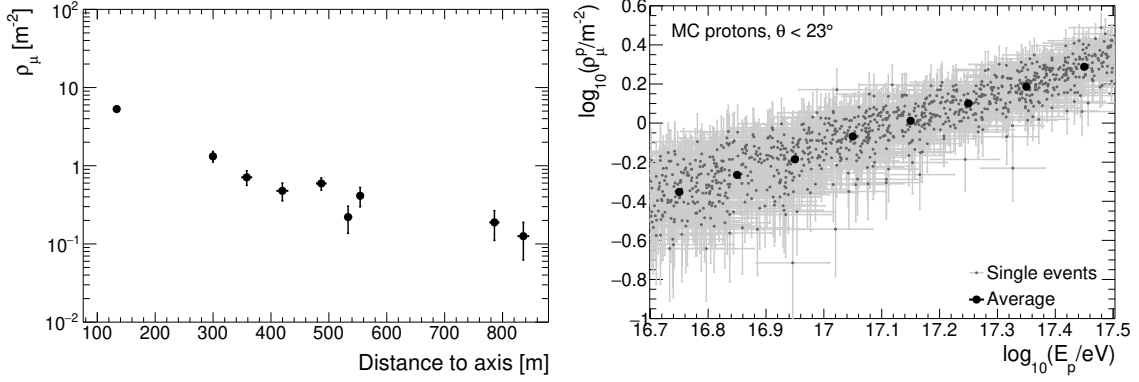tions. An example of an acquired event is illustrated in Fig. 3 (left). We define the event-based observable M_b using the measured muon density ρ_μ^i at a distance r_i from the shower axis [12]:

$$M_b = \log_{10}\left(\sum_i \frac{\rho_\mu^i}{\rho_\mu^\mathrm{p}} \times \left(\frac{r_i}{200\,\mathrm{m}}\right)^b\right) \tag{2}$$

The choice of $b = 1$ has been found to provide the best separation power between photons and protons at tens of PeV. The discrimination observable M_b is characterized with the simulated events described before. A reference distance of 200 m is chosen based on the fluctuations in the number of muons. These relative fluctuations exhibit a minimum plateau between 50 and 300 m in the energy range relevant to this work. Beyond this range, the uncertainties increase rapidly due to the inherent Poissonian fluctuations associated with the decreasing number of muons. The normalization factor ρ_μ^p is defined as the average muon density at 200 m from the shower axis in simulated proton events. This quantity is parameterized using an unbinned maximum likelihood approach, as illustrated in Fig. 3 (right). The likelihood model accounts for the zenith-dependent atmospheric attenuation of the muon component. As a result, events from hadronic origin would typically yield positive values of M_b, while events with photon origin exhibit negative values (Fig. 4, left).

The energy reconstruction method optimized for hadronic showers tends to underestimate the energy in the case of photon primaries due to their delayed shower development and the lack of a significant muon component. Still, a single energy scale needs to be employed for all events, irrespective of the primary particle species. As a solution, a photon energy scale is customized. It consists of an attenuation function, f_att, parameterized using simulated proton events, and an energy

Figure 3: Left: The lateral distribution of muons as measured by the UMD stations in terms of the distance to the shower axis for a measured event of $\theta = 7.7 \pm 0.4\,^\circ$ and a reconstructed hadronic energy of $E = (2.54 \pm 0.09) \times 10^{17}$ eV. Right: The simulated muon density at 200 m from the shower axis for proton-initiated showers of zenith angle $\theta < 23\,^\circ$ as a function of the reconstructed energy.

calibration specific to photon events, represented by the parameters E_0 and α. Given the signal obtained from the WCDs at 250 m from the shower axis, S_{250}, and the reconstructed zenith angle θ, the photon energy scale is defined as:

$$S_{250} = f_{\text{att}}(\theta) \times \left(\frac{E_\gamma}{E_0}\right)^\alpha \tag{3}$$

The energy bias for proton events with respect to a dedicated energy calibration finely tuned with simulations is +8%, accounting for the employed energy parameters E_0 and α in Eq. 3. In the case of data, the energy bias with respect to the calorimetric energy scale extrapolated from fluorescence measurements above 100 PeV [8] is +33%. Within a given E_γ bin, photon events are mixed with proton events having lower energies. This ensures that the discrimination method is tuned within a conservative scenario, where the risk of misidentifying simulated proton as photon events is minimized.

In Fig. 4 (left), the simulated distributions of photon and proton events within the energy range $16.7 < \log_{10}(E_\gamma/\text{eV}) < 16.9$ are displayed. A minor population of photon showers with a hadronic-like muon content is seen, corresponding to a leading $\pi^\pm$ at the early stages of development. The discrimination power of the method is evaluated based on the background contamination, which refers to the presence of background events below the photon candidate cut. The photon candidate cut is determined as the median of the M_b distribution for simulated photon events.

To estimate the contamination, the 10% most photon-like background events are fitted with an unbinned maximum likelihood procedure assuming an exponential model. The contamination is then determined by calculating the fraction of the fitted tail to the left of the candidate cut. This fraction, as depicted in Fig. 4 (right), for the north-west hexagon, is found to be less than 10^{-5} when considering a pure proton background and 50% signal efficiency as reference.

It is worth noting that M_b scales by definition with the number of available UMD stations. Moreover, the background contamination tends to increase when two neighboring first-crown UMD stations are missing in an event. This can occur due to the absence of deployed UMD stations or
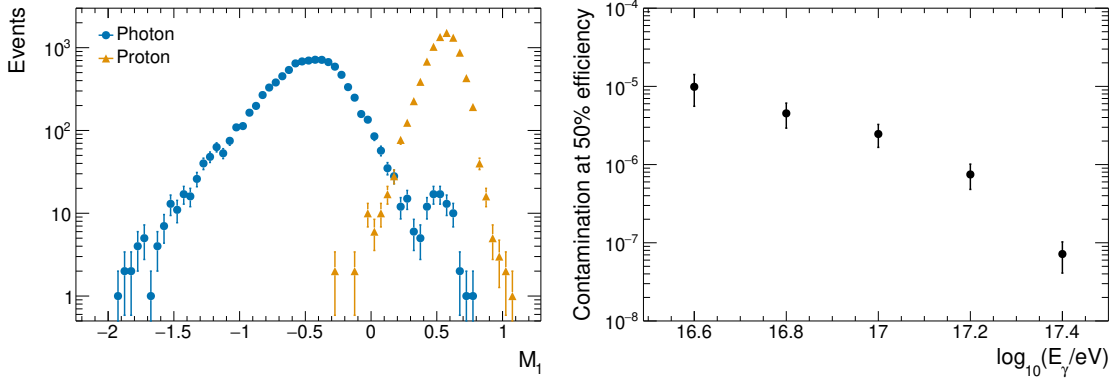
Figure 4: Left: The $M_{b=1}$ distributions for photon- and proton-initiated events for energies $16.7 < \log_{10}(E_\gamma/\text{eV}) < 16.9$ and $\theta < 52°$. Right: The background contamination at a fixed 50% signal efficiency in terms of the photon energy E_γ.

technical issues with either the WCD or the UMD station itself. Consequently, the background contamination profile and the photon candidate cut are deduced for each possible combination of the number of first-crown UMD stations and their relative positions.

4. Application of the method to the data

The background contamination profiles (Fig. 4, right), are parameterized as a function of the photon energy. This allows for the assignment of a probability to each hadronic event, indicating the likelihood of it being misidentified as a photon candidate under the conservative assumption of a pure-proton background. By estimating the expected number of background events incorrectly labeled as photon candidates, it becomes possible to anticipate the presence of such events before unblinding the complete search data-set.

The maximum expected number of fake photon events for the fully-operational north-west hexagon is depicted in Fig. 5 (left). The number of fake photon events above $10^{16.7}$ eV in the corresponding sub-set comprised by 3295 events is $(4.04 \pm 0.04) \times 10^{-3}$. This is translated to an average occurrence of one fake photon event approximately every 815, 650 events. Considering that this hexagon was fully-operational during ∼10 months of the observation time, one fake photon is expected every 106 years of operation with ideal uptime.

Given the low probability of observing an event consistent with the photon hypothesis, ∼10% of the selected data for each hexagon is burnt to check the M_b distributions: in Fig. 5 (right), the energy-integrated distributions of simulated events, weighted by E_γ^{-2}, are displayed alongside the burnt M_b distribution without any energy-weighting for the fully-operative north-west hexagon.

The remaining ∼90% of the data are unblinded and the M_b distributions are compared to the photon candidate cut. No photon candidates are identified. As a result, upper limits to the integral photon flux are computed using the Feldman-Cousins approach [13] at 95% confidence level as 12.04, 11.02, 10.67 and 10.61 km^{-2} sr^{-1} yr^{-1} above threshold energies of 50, 80, 120 and 200 PeV.

Possible systematic effects that could influence the upper limits have been carefully studied. These include variations in the muon counting strategy used to convert digital traces to the number
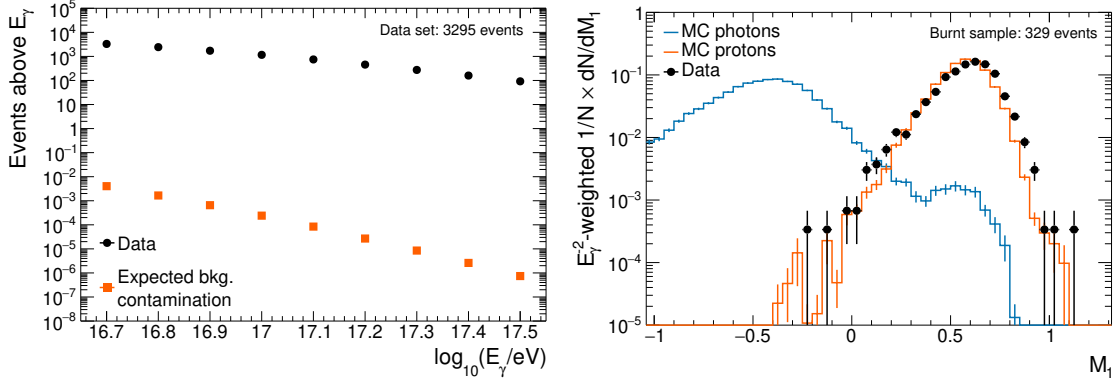
Figure 5: Left: The integral number of events and the estimated number of events coming from the expected background contamination in terms of the minimum energy. Right: The $M_{b=1}$ distributions for simulated proton and photon events weighted by E^{-2} for energies above $E_\gamma = 10^{16.7}$ eV. Black markers represent the burnt data composed of 329 events. In both panels, events acquired with the fully-operative northwest hexagon are considered.

of muons in the UMD stations, uncertainties in the soil shielding arising from the varying soil density in the Auger site, and uncertainties from the available hadronic models. In the most extreme case, the values of ρ_μ in the data may be decreased by up to 13%. However, even with this significant decrease, no events fall below the photon candidate cut. Regarding the exposure, the relative uncertainty of the event rate, the inherent energy bias in data when using the photonic energy scale, and a change in the photon spectral index between $\gamma = -2$ and $\gamma = -3$ are translated into a global systematic uncertainty of $(-33.7\%; +4.07\%)$.

In Fig. 6, we present the upper limits on the integral photon flux obtained in this study (represented by red markers), along with the limits previously reported by Auger and other experiments [14]. Notably, the limits derived in this work are the most stringent in the energy range between 50 and 200 PeV. In this way, the Auger photon search programme has been extended to cover more than three decades in the cosmic-ray energy spectrum. Furthermore, the exposure accumulated by Auger until 2035 would provide enough sensitivity (light red line) to put constraints in the mass-lifetime phase-space for specific dark matter models (dashed lines), as well as to explore the expected photon flux from pp interactions in the Galactic halo.

5. Conclusions

This study represents the first search for a diffuse flux of primary photons from the Southern Hemisphere at energies between 50 and 200 PeV. Leveraging the densest surface array and the underground muon detectors of the Pierre Auger Observatory, a high-quality data-set comprising over 15,000 events above 50 PeV was analyzed. No event compatible with a photon origin was observed in this data-set. Consequently, upper limits to the integral photon flux were established above 50 to 200 PeV, with values ranging from 10.61 to 12.04 km^{-2} sr^{-1} yr^{-1}. These limits were derived based on an exposure equivalent to approximately eight months of ideal operation. Finally, the expected exposure accumulated until 2035 is anticipated to offer a significant opportunity to test
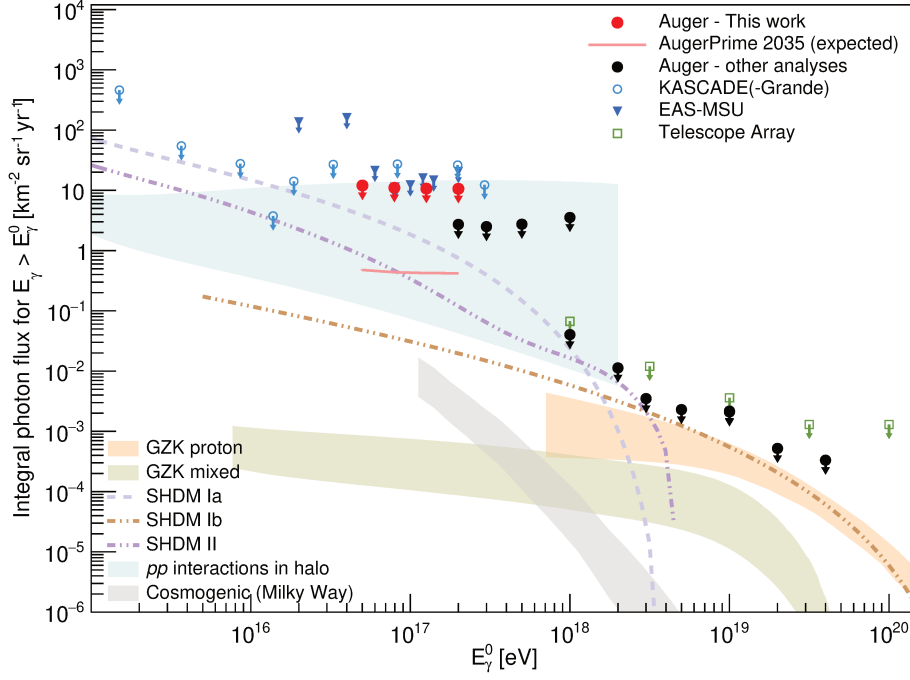
Figure 6: The upper limits to the integral photon flux obtained in this work, as solid red markers, limits obtained by Auger at higher energies [6], as solid black markers, compared to limits reported by other experiments [14]. Bands correspond to the predicted cosmogenic photon fluxes [2–4, 15]. Dashed lines correspond to super-heavy dark matter predictions: (decay into hadrons) $M_X = 10^{10}$ GeV and a lifetime $\tau_X = 3 \times 10^{21}$ yr [16] in blue; $M_X = 10^{12}$ GeV and a lifetime $\tau_X = 10^{23}$ yr [16] in brown; (decay into leptons) $M_X = 10^{10}$ GeV and a lifetime $\tau_X = 3 \times 10^{21}$ yr [5] in purple. The light red line symbolizes the expected sensitivity with the exposure accumulated until 2035.

the predicted photon flux from various models about super-heavy dark matter and pp interactions in the Galactic halo in the tens of PeV energy range.

References

[1] Z. Cao *et al.* [LHAASO Coll.], Nature **594** (2021) 33.

[2] C. Bérat, C. Bleve, O. Deligny, F. Montanet, P. Savina and Z. Torrès, Astrophys. J. **929** (2022) 55 [2203.08751].

[3] K.-H. Kampert, B. Sarkar, J. Kulbartz, L. Maccione, N. Nierstenhoefer and G. Sigl, ICRC (Beijing) **2** (2011) 198.

[4] A. Bobrikova, M. Niechciol, M. Risse and P. Ruehl, ICRC (Berlin) **395** (2021) 449.

[5] M. Kachelriess, O.E. Kalashev and M.Y. Kuznetsov, Phys. Rev. D **98** (2018) 083016 [1805.04500].

[6] M. Niechciol *et al.* [Pierre Auger Coll.], these proceedings, Proc. of Science **444** (2023) 1488.

[7] A. Castellina *et al.* [Pierre Auger Coll.], EPJ Web of Conf. **210** (2019) 06002 [1905.04472].

[8] G. Brichetto *et al.* [Pierre Auger Coll.], these proceedings, Proc. of Science **444** (2023) 398.

[9] J. de Jesus *et al.* [Pierre Auger Coll.], these proceedings, Proc. of Science **444** (2023) 267.

[10] W.D. Apel *et al.* [KASCADE-Grande Coll.], Astrophys. J. **848** (2017) 1 [1710.02889].

[11] E. Santos *et al.* [Pierre Auger Coll.], these proceedings, Proc. of Science **444** (2023) 248.

[12] N. González, F. Sánchez, M. Roth and A. Etchegoyen, Astropart. Phys. **114** (2020) 48.

[13] G.J. Feldman and R.D. Cousins, Phys. Rev. D **57** (1998) 3873 [9711021].

[14] P. Abreu *et al.* [Pierre Auger Coll.], Universe **8** (2022) 579 [2210.12959].

[15] O.E. Kalashev and S.V. Troitsky, Pisma Zh. Eksp. Teor. Fiz. **100** (2014) 865 [1410.2600].

[16] O.K. Kalashev and M.Y. Kuznetsov, Phys. Rev. D **94** (2016) 063535 [1606.07354].

The Pierre Auger Collaboration

A. Abdul Halim[13], P. Abreu[72], M. Aglietta[54,52], I. Allekotte[1], K. Almeida Cheminant[70], A. Almela[7,12], R. Aloisio[45,46], J. Alvarez-Muñiz[79], J. Ammerman Yebra[79], G.A. Anastasi[54,52], L. Anchordoqui[86], B. Andrada[7], S. Andringa[72], C. Aramo[50], P.R. Araújo Ferreira[42], E. Arnone[63,52], J. C. Arteaga Velázquez[67], H. Asorey[7], P. Assis[72], G. Avila[11], E. Avocone[57,46], A.M. Badescu[75], A. Bakalova[32], A. Balaceanu[73], F. Barbato[45,46], A. Bartz Mocellin[85], J.A. Bellido[13,69], C. Berat[36], M.E. Bertaina[63,52], G. Bhatta[70], M. Bianciotto[63,52], P.L. Biermann[h], V. Binet[5], K. Bismark[39,7], T. Bister[80,81], J. Biteau[37], J. Blazek[32], C. Bleve[36], J. Blümer[41], M. Boháčová[32], D. Boncioli[57,46], C. Bonifazi[8,26], L. Bonneau Arbeletche[21], N. Borodai[70], J. Brack[j], P.G. Brichetto Orchera[7], F.L. Briechle[42], A. Bueno[78], S. Buitink[15], M. Buscemi[47,61], M. Büsken[39,7], A. Bwembya[80,81], K.S. Caballero-Mora[66], S. Cabana-Freire[79], L. Caccianiga[59,49], I. Caracas[38], R. Caruso[58,47], A. Castellina[54,52], F. Catalani[18], G. Cataldi[48], L. Cazon[79], M. Cerda[10], A. Cermenati[45,46], J.A. Chinellato[21], J. Chudoba[32], L. Chytka[33], R.W. Clay[13], A.C. Cobos Cerutti[6], R. Colalillo[60,50], A. Coleman[90], M.R. Coluccia[48], R. Conceição[72], A. Condorelli[37], G. Consolati[49,55], M. Conte[56,48], F. Convenga[41], D. Correia dos Santos[28], P.J. Costa[72], C.E. Covault[84], M. Cristinziani[44], C.S. Cruz Sanchez[3], S. Dasso[4,2], K. Daumiller[41], B.R. Dawson[13], R.M. de Almeida[28], J. de Jesús[7,41], S.J. de Jong[80,81], J.R.T. de Mello Neto[26,27], I. De Mitri[45,46], J. de Oliveira[17], D. de Oliveira Franco[21], F. de Palma[56,48], V. de Souza[19], E. De Vito[56,48], A. Del Popolo[58,47], O. Deligny[34], N. Denner[32], L. Deval[41,7], A. di Matteo[52], M. Dobre[73], C. Dobrigkeit[21], J.C. D'Olivo[68], L.M. Domingues Mendes[72], J.C. dos Anjos, R.C. dos Anjos[25], J. Ebr[32], F. Ellwanger[41], M. Emam[80,81], R. Engel[39,41], I. Epicoco[56,48], M. Erdmann[42], A. Etchegoyen[7,12], C. Evoli[45,46], H. Falcke[80,82,81], J. Farmer[89], G. Farrar[88], A.C. Fauth[21], N. Fazzini[e], F. Feldbusch[40], F. Fenu[41,d], A. Fernandes[72], B. Fick[87], J.M. Figueira[7], A. Filipčič[77,76], T. Fitoussi[41], B. Flaggs[90], T. Fodran[80], T. Fujii[89,f], A. Fuster[7,12], C. Galea[80], C. Galelli[59,49], B. García[6], C. Gaudu[38], H. Gemmeke[40], F. Gesualdi[7,41], A. Gherghel-Lascu[73], P.L. Ghia[34], U. Giaccari[48], M. Giammarchi[49], J. Glombitza[42,g], F. Gobbi[10], F. Gollan[7], G. Golup[1], M. Gómez Berisso[1], P.F. Gómez Vitale[11], J.P. Gongora[11], J.M. González[1], N. González[7], I. Goos[1], D. Góra[70], A. Gorgi[54,52], M. Gottowik[79], T.D. Grubb[13], F. Guarino[60,50], G.P. Guedes[22], E. Guido[44], S. Hahn[39], P. Hamal[32], M.R. Hampel[7], P. Hansen[3], D. Harari[1], V.M. Harvey[13], A. Haungs[41], T. Hebbeker[42], C. Hojvat[e], J.R. Hörandel[80,81], P. Horvath[33], M. Hrabovský[33], T. Huege[41,15], A. Insolia[58,47], P.G. Isar[74], P. Janecek[32], J.A. Johnsen[85], J. Jurysek[32], A. Kääpä[38], K.H. Kampert[38], B. Keilhauer[41], A. Khakurdikar[80], V.V. Kizakke Covilakam[7,41], H.O. Klages[41], M. Kleifges[40], F. Knapp[39], N. Kunka[40], B.L. Lago[16], N. Langner[42], M.A. Leigui de Oliveira[24], Y Lema-Capeans[79], V. Lenok[39], A. Letessier-Selvon[35], I. Lhenry-Yvon[34], D. Lo Presti[58,47], L. Lopes[72], L. Lu[91], Q. Luce[39], J.P. Lundquist[76], A. Machado Payeras[21], M. Majercakova[32], D. Mandat[32], B.C. Manning[13], P. Mantsch[e], S. Marafico[34], F.M. Mariani[59,49], A.G. Mariazzi[3], I.C. Mariş[14], G. Marsella[61,47], D. Martello[56,48], S. Martinelli[41,7], O. Martínez Bravo[64], M.A. Martins[79], M. Mastrodicasa[57,46], H.J. Mathes[41], J. Matthews[a], G. Matthiae[62,51], E. Mayotte[85,38], S. Mayotte[85], P.O. Mazur[e], G. Medina-Tanco[68], J. Meinert[38], D. Melo[7], A. Menshikov[40], C. Merx[41], S. Michal[33], M.I. Micheletti[5], L. Miramonti[59,49], S. Mollerach[1], F. Montanet[36], L. Morejon[38], C. Morello[54,52], A.L. Müller[32], K. Mulrey[80,81], R. Mussa[52], M. Muzio[88], W.M. Namasaka[38], S. Negi[32], L. Nellen[68], K. Nguyen[87], G. Nicora[9], M. Niculescu-Oglinzanu[73], M. Niechciol[44], D. Nitz[87], D. Nosek[31], V. Novotny[31], L. Nožka[33], A Nucita[56,48], L.A. Núñez[30], C. Oliveira[19], M. Palatka[32], J. Pallotta[9], S. Panja[32], G. Parente[79], T. Paulsen[38], J. Pawlowsky[38], M. Pech[32], J. Pękala[70], R. Pelayo[65], L.A.S. Pereira[23], E.E. Pereira Martins[39,7], J. Perez Armand[20], C. Pérez Bertolli[7,41], L. Perrone[56,48], S. Petrera[45,46], C. Petrucci[57,46], T. Pierog[41], M. Pimenta[72], M. Platino[7], B. Pont[80], M. Pothast[81,80], M. Pourmohammad Shahvar[61,47], P. Privitera[89], M. Prouza[32], A. Puyleart[87], S. Querchfeld[38], J. Rautenberg[38], D. Ravignani[7], M. Reininghaus[39], J. Ridky[32], F. Riehn[79], M. Risse[44], V. Rizi[57,46], W. Rodrigues de Carvalho[80], E. Rodriguez[7,41], J. Rodriguez Rojo[11], M.J. Roncoroni[7], S. Rossoni[43], M. Roth[41], E. Roulet[1], A.C. Rovero[4], P. Ruehl[44], A. Saftoiu[73], M. Saharan[80], F. Salamida[57,46], H. Salazar[64], G. Salina[51], J.D. Sanabria Gomez[30], F. Sánchez[7], E.M. Santos[20], E. Santos[32],

F. Sarazin[85], R. Sarmento[72], R. Sato[11], P. Savina[91], C.M. Schäfer[41], V. Scherini[56,48], H. Schieler[41], M. Schimassek[34], M. Schimp[38], F. Schlüter[41], D. Schmidt[39], O. Scholten[15,i], H. Schoorlemmer[80,81], P. Schovánek[32], F.G. Schröder[90,41], J. Schulte[42], T. Schulz[41], S.J. Sciutto[3], M. Scornavacche[7,41], A. Segreto[53,47], S. Sehgal[38], S.U. Shivashankara[76], G. Sigl[43], G. Silli[7], O. Sima[73,b], F. Simon[40], R. Smau[73], R. Šmída[89], P. Sommers[k], J.F. Soriano[86], R. Squartini[10], M. Stadelmaier[32], D. Stanca[73], S. Stanič[76], J. Stasielak[70], P. Stassi[36], S. Strähnz[39], M. Straub[42], M. Suárez-Durán[14], T. Suomijärvi[37], A.D. Supanitsky[7], Z. Svozilikova[32], Z. Szadkowski[71], A. Tapia[29], C. Taricco[63,52], C. Timmermans[81,80], O. Tkachenko[41], P. Tobiska[32], C.J. Todero Peixoto[18], B. Tomé[72], Z. Torrès[36], A. Travaini[10], P. Travnicek[32], C. Trimarelli[57,46], M. Tueros[3], M. Unger[41], L. Vaclavek[33], M. Vacula[33], J.F. Valdés Galicia[68], L. Valore[60,50], E. Varela[64], A. Vásquez-Ramírez[30], D. Veberič[41], C. Ventura[27], I.D. Vergara Quispe[3], V. Verzi[51], J. Vicha[32], J. Vink[83], J. Vlastimil[32], S. Vorobiov[76], C. Watanabe[26], A.A. Watson[c], A. Weindl[41], L. Wiencke[85], H. Wilczyński[70], D. Wittkowski[38], B. Wundheiler[7], B. Yue[38], A. Yushkov[32], O. Zapparrata[14], E. Zas[79], D. Zavrtanik[76,77], M. Zavrtanik[77,76]

──────── • ────────

[1] Centro Atómico Bariloche and Instituto Balseiro (CNEA-UNCuyo-CONICET), San Carlos de Bariloche, Argentina

[2] Departamento de Física and Departamento de Ciencias de la Atmósfera y los Océanos, FCEyN, Universidad de Buenos Aires and CONICET, Buenos Aires, Argentina

[3] IFLP, Universidad Nacional de La Plata and CONICET, La Plata, Argentina

[4] Instituto de Astronomía y Física del Espacio (IAFE, CONICET-UBA), Buenos Aires, Argentina

[5] Instituto de Física de Rosario (IFIR) – CONICET/U.N.R. and Facultad de Ciencias Bioquímicas y Farmacéuticas U.N.R., Rosario, Argentina

[6] Instituto de Tecnologías en Detección y Astropartículas (CNEA, CONICET, UNSAM), and Universidad Tecnológica Nacional – Facultad Regional Mendoza (CONICET/CNEA), Mendoza, Argentina

[7] Instituto de Tecnologías en Detección y Astropartículas (CNEA, CONICET, UNSAM), Buenos Aires, Argentina

[8] International Center of Advanced Studies and Instituto de Ciencias Físicas, ECyT-UNSAM and CONICET, Campus Miguelete – San Martín, Buenos Aires, Argentina

[9] Laboratorio Atmósfera – Departamento de Investigaciones en Láseres y sus Aplicaciones – UNIDEF (CITEDEF-CONICET), Argentina

[10] Observatorio Pierre Auger, Malargüe, Argentina

[11] Observatorio Pierre Auger and Comisión Nacional de Energía Atómica, Malargüe, Argentina

[12] Universidad Tecnológica Nacional – Facultad Regional Buenos Aires, Buenos Aires, Argentina

[13] University of Adelaide, Adelaide, S.A., Australia

[14] Université Libre de Bruxelles (ULB), Brussels, Belgium

[15] Vrije Universiteit Brussels, Brussels, Belgium

[16] Centro Federal de Educação Tecnológica Celso Suckow da Fonseca, Petropolis, Brazil

[17] Instituto Federal de Educação, Ciência e Tecnologia do Rio de Janeiro (IFRJ), Brazil

[18] Universidade de São Paulo, Escola de Engenharia de Lorena, Lorena, SP, Brazil

[19] Universidade de São Paulo, Instituto de Física de São Carlos, São Carlos, SP, Brazil

[20] Universidade de São Paulo, Instituto de Física, São Paulo, SP, Brazil

[21] Universidade Estadual de Campinas, IFGW, Campinas, SP, Brazil

[22] Universidade Estadual de Feira de Santana, Feira de Santana, Brazil

[23] Universidade Federal de Campina Grande, Centro de Ciencias e Tecnologia, Campina Grande, Brazil

[24] Universidade Federal do ABC, Santo André, SP, Brazil

[25] Universidade Federal do Paraná, Setor Palotina, Palotina, Brazil

[26] Universidade Federal do Rio de Janeiro, Instituto de Física, Rio de Janeiro, RJ, Brazil

[27] Universidade Federal do Rio de Janeiro (UFRJ), Observatório do Valongo, Rio de Janeiro, RJ, Brazil

[28] Universidade Federal Fluminense, EEIMVR, Volta Redonda, RJ, Brazil

[29] Universidad de Medellín, Medellín, Colombia

[30] Universidad Industrial de Santander, Bucaramanga, Colombia

[31] Charles University, Faculty of Mathematics and Physics, Institute of Particle and Nuclear Physics, Prague, Czech Republic

[32] Institute of Physics of the Czech Academy of Sciences, Prague, Czech Republic

[33] Palacky University, Olomouc, Czech Republic

[34] CNRS/IN2P3, IJCLab, Université Paris-Saclay, Orsay, France

[35] Laboratoire de Physique Nucléaire et de Hautes Energies (LPNHE), Sorbonne Université, Université de Paris, CNRS-IN2P3, Paris, France

[36] Univ. Grenoble Alpes, CNRS, Grenoble Institute of Engineering Univ. Grenoble Alpes, LPSC-IN2P3, 38000 Grenoble, France

[37] Université Paris-Saclay, CNRS/IN2P3, IJCLab, Orsay, France

[38] Bergische Universität Wuppertal, Department of Physics, Wuppertal, Germany

[39] Karlsruhe Institute of Technology (KIT), Institute for Experimental Particle Physics, Karlsruhe, Germany

[40] Karlsruhe Institute of Technology (KIT), Institut für Prozessdatenverarbeitung und Elektronik, Karlsruhe, Germany

[41] Karlsruhe Institute of Technology (KIT), Institute for Astroparticle Physics, Karlsruhe, Germany

[42] RWTH Aachen University, III. Physikalisches Institut A, Aachen, Germany

[43] Universität Hamburg, II. Institut für Theoretische Physik, Hamburg, Germany

[44] Universität Siegen, Department Physik – Experimentelle Teilchenphysik, Siegen, Germany

[45] Gran Sasso Science Institute, L'Aquila, Italy

[46] INFN Laboratori Nazionali del Gran Sasso, Assergi (L'Aquila), Italy

[47] INFN, Sezione di Catania, Catania, Italy

[48] INFN, Sezione di Lecce, Lecce, Italy

[49] INFN, Sezione di Milano, Milano, Italy

[50] INFN, Sezione di Napoli, Napoli, Italy

[51] INFN, Sezione di Roma "Tor Vergata", Roma, Italy

[52] INFN, Sezione di Torino, Torino, Italy

[53] Istituto di Astrofisica Spaziale e Fisica Cosmica di Palermo (INAF), Palermo, Italy

[54] Osservatorio Astrofisico di Torino (INAF), Torino, Italy

[55] Politecnico di Milano, Dipartimento di Scienze e Tecnologie Aerospaziali , Milano, Italy

[56] Università del Salento, Dipartimento di Matematica e Fisica "E. De Giorgi", Lecce, Italy

[57] Università dell'Aquila, Dipartimento di Scienze Fisiche e Chimiche, L'Aquila, Italy

[58] Università di Catania, Dipartimento di Fisica e Astronomia "Ettore Majorana", Catania, Italy

[59] Università di Milano, Dipartimento di Fisica, Milano, Italy

[60] Università di Napoli "Federico II", Dipartimento di Fisica "Ettore Pancini", Napoli, Italy

[61] Università di Palermo, Dipartimento di Fisica e Chimica "E. Segrè", Palermo, Italy

[62] Università di Roma "Tor Vergata", Dipartimento di Fisica, Roma, Italy

[63] Università Torino, Dipartimento di Fisica, Torino, Italy

[64] Benemérita Universidad Autónoma de Puebla, Puebla, México

[65] Unidad Profesional Interdisciplinaria en Ingeniería y Tecnologías Avanzadas del Instituto Politécnico Nacional (UPIITA-IPN), México, D.F., México

[66] Universidad Autónoma de Chiapas, Tuxtla Gutiérrez, Chiapas, México

[67] Universidad Michoacana de San Nicolás de Hidalgo, Morelia, Michoacán, México

[68] Universidad Nacional Autónoma de México, México, D.F., México

[69] Universidad Nacional de San Agustin de Arequipa, Facultad de Ciencias Naturales y Formales, Arequipa, Peru

[70] Institute of Nuclear Physics PAN, Krakow, Poland

[71] University of Łódź, Faculty of High-Energy Astrophysics,Łódź, Poland

[72] Laboratório de Instrumentação e Física Experimental de Partículas – LIP and Instituto Superior Técnico – IST, Universidade de Lisboa – UL, Lisboa, Portugal

[73] "Horia Hulubei" National Institute for Physics and Nuclear Engineering, Bucharest-Magurele, Romania

[74] Institute of Space Science, Bucharest-Magurele, Romania

[75] University Politehnica of Bucharest, Bucharest, Romania

[76] Center for Astrophysics and Cosmology (CAC), University of Nova Gorica, Nova Gorica, Slovenia

[77] Experimental Particle Physics Department, J. Stefan Institute, Ljubljana, Slovenia

[78] Universidad de Granada and C.A.F.P.E., Granada, Spain

[79] Instituto Galego de Física de Altas Enerxías (IGFAE), Universidade de Santiago de Compostela, Santiago de Compostela, Spain

[80] IMAPP, Radboud University Nijmegen, Nijmegen, The Netherlands

[81] Nationaal Instituut voor Kernfysica en Hoge Energie Fysica (NIKHEF), Science Park, Amsterdam, The Netherlands

[82] Stichting Astronomisch Onderzoek in Nederland (ASTRON), Dwingeloo, The Netherlands

[83] Universiteit van Amsterdam, Faculty of Science, Amsterdam, The Netherlands

[84] Case Western Reserve University, Cleveland, OH, USA

[85] Colorado School of Mines, Golden, CO, USA

[86] Department of Physics and Astronomy, Lehman College, City University of New York, Bronx, NY, USA

[87] Michigan Technological University, Houghton, MI, USA

[88] New York University, New York, NY, USA

[89] University of Chicago, Enrico Fermi Institute, Chicago, IL, USA

[90] University of Delaware, Department of Physics and Astronomy, Bartol Research Institute, Newark, DE, USA

[91] University of Wisconsin-Madison, Department of Physics and WIPAC, Madison, WI, USA

——

[a] Louisiana State University, Baton Rouge, LA, USA

[b] also at University of Bucharest, Physics Department, Bucharest, Romania

[c] School of Physics and Astronomy, University of Leeds, Leeds, United Kingdom

[d] now at Agenzia Spaziale Italiana (ASI). Via del Politecnico 00133, Roma, Italy

[e] Fermi National Accelerator Laboratory, Fermilab, Batavia, IL, USA

[f] now at Graduate School of Science, Osaka Metropolitan University, Osaka, Japan

[g] now at ECAP, Erlangen, Germany

[h] Max-Planck-Institut für Radioastronomie, Bonn, Germany

[i] also at Kapteyn Institute, University of Groningen, Groningen, The Netherlands

[j] Colorado State University, Fort Collins, CO, USA

[k] Pennsylvania State University, University Park, PA, USA

Acknowledgments